

MMA Memo: 062

An Independent Simulation of Imaging Characteristics of a Millimetre Array, with and without a single Large Element (LE), and a LE pointing correction algorithm

D.T. Emerson,

NRAO, Tucson.

November 25, 1990
(Posted October 1998)

Abstract

As part of the MMA imaging group's investigations into the MMA imaging characteristics, a study has been made of imaging characteristics of a Millimeter Array consisting of a large number of 8m antennas, in which short spacing information is obtained either from the 8m array elements operating in single dish mode, or from a separate 20m dish. This study overlaps with some of the work of earlier studies (refs (1), (2), (3) and other references therein) and gives an independent confirmation of some of that work. The current study examines in more detail the relative importance of different components of the pointing error model, and presents an algorithm (PHFIT) which may lead to a relaxation of pointing requirements of the individual antennas.

The conclusions are summarized as:

1. Where similar parameters of noise and pointing errors have been used there is good agreement with earlier work (refs (1),(2))
2. Independent investigation of different pointing error components (global, differential systematic, random) shows that the dominant components regarding degradation of dynamic range after single dish and MMA interferometric data have been combined are:
 - (a) For single dish data, using either the 8m elements in total power or a separate 20m large element (LE), global map pointing offsets.
 - (b) For interferometric measurements, the differential systematic pointing error, i.e. the mean pointing error in the relative offset of one field of the mosaic with respect to its neighbours, is the dominant source of error.

A given uncorrected pointing error in short spacing data, derived either from a 20m or an 8m antenna element, is more harmful than the same pointing affecting interferometric data, by a factor typically of 4 to 6, depending on circumstances. If not corrected, a given global pointing error on 20m single dish is much more harmful than the same angular pointing error on an 8m dish. Purely random errors, such as tracking errors, are less important.

3. The effect of the global pointing error of single dish observations, either with the 8m dishes or a separate 20m dish providing the short-spacing data, can effectively be eliminated by making use of the overlap in the UV plane of regions common to both single dish and interferometric data. This technique is very effective, and probably should be applied as a standard correction to most combined single dish and interferometric data sets. In the presence of a poor signal-to-noise ratio, the technique degrades more rapidly with a smaller single dish and its smaller area of UV plane overlap with interferometric data, than with a large single dish element.
4. If the phase overlap correction technique is applied, the 20m single dish always gives greater dynamic range in the combined MMA image than a corresponding 8m dish in total power mode. However, the difference is often marginal.

Introduction

Some extensive investigations into mosaicing and the imaging properties of the proposed MMA have already been carried out (refs (1),(2),(3)). Work reported here supplements these earlier investigations, examining in more detail the comparison between arrays with and without an extra single large element (LE), in the presence of different types of pointing error and in the presence of noise. Simulations were carried out using the same model source as the earlier investigations, but with software developed independently. Because of the importance of results derived from simulations to the design specifications of the MMA, it was thought useful to verify some aspects of the earlier simulations with independent software and starting with different initial assumptions.

Description of the Simulations

The simulations described here are equivalent to an ideal linear mosaic analysis of data. The model source, shown in Fig (1), is the same as was used in earlier simulations. Here, the model is represented by a 128 by 128 grid, sampled at 1" intervals, i.e. a total extent of ~2.1 arc min. The assumed wavelength is 1.3 mm. The region of emission extends over ~1.5' within this field. Observations were simulated using a MMA with 8m diameter antenna elements, with interferometer spacings range from 9m to 70m. Short spacing information is provided either by the 8m elements operating independently, not simultaneously, in total power mode, or by a separate 20m diameter single dish. The 8m and 20m elements were given a gaussian illumination taper truncated at -12 dB at the edge of each dish. The effect of varying the degree of taper was investigated, but only very minor variations on the results of the simulations were found. The beamwidth (fwhp) of an 8m dish at 1.3mm is ~40", and of a 20m dish ~16". The polar diagram of the interferometer dishes was truncated in the simulations at the first null, a radius of 50". The nominal mosaic pointing centres of the interferometer array were spaced at 16" intervals, with some tests varying this spacing. The data were well sampled in the UV plane, and the synthesized beam was assumed to be identical at all parts of the mosaiced field. For some tests various amounts of noise was added. In most tests, the same UV plane rms noise level was used for single dish data as for the interferometric data.

Dynamic range was used as a measure of quality of the mosaic reconstruction. Dynamic range is defined here as the ratio of the peak brightness of the model data to the rms value of the residual map (model data - simulated reconstruction), with both model and reconstruction truncated at the same radius in the UV plane. The absolute value of the dynamic range is highly dependent on details of the model source, its extent within the total field, and the maximum interferometric baseline used for the simulated reconstruction. However, values of this parameter are a good measure of the **relative** importance of different sources of error.

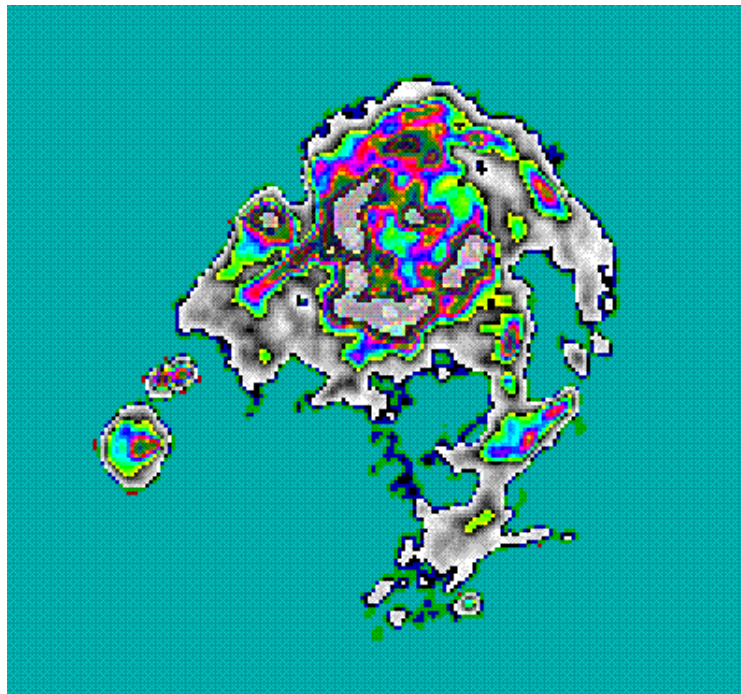


Figure 1: The raw data used for these simulations. The total extent of the field is 2.1 arc min.

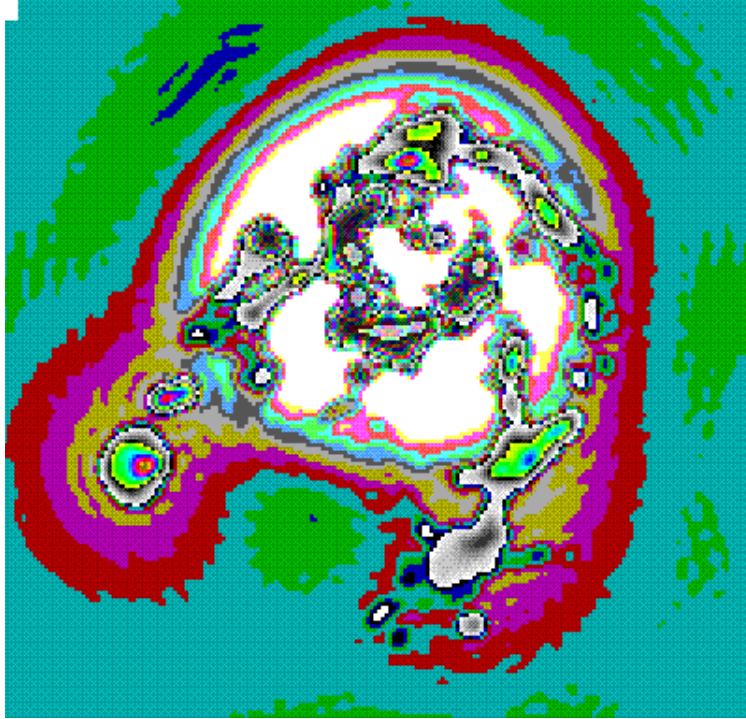


Figure 2: The raw data shown in Figure 1, observed with the MMA, but without any short spacing information. The maximum interferometer baseline is 70m, the minimum 9m, with 8m antennas are assumed for the simulated observations.

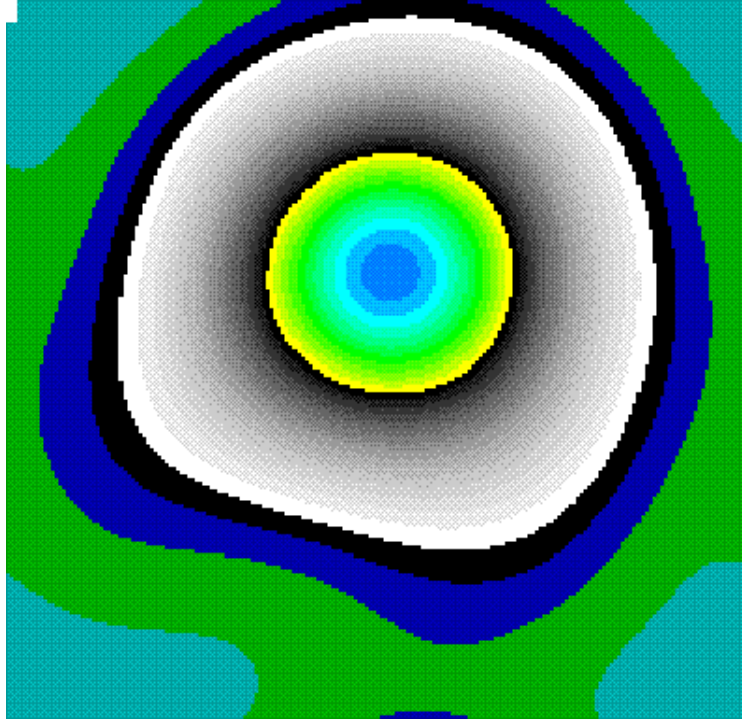


Figure 3: The data of Figure 1 as it would appear observed with an 8m dish in total power. This information, or that of Figure 4, is used to supplement Figure 2 to give the final simulated result shown in Figure 5.

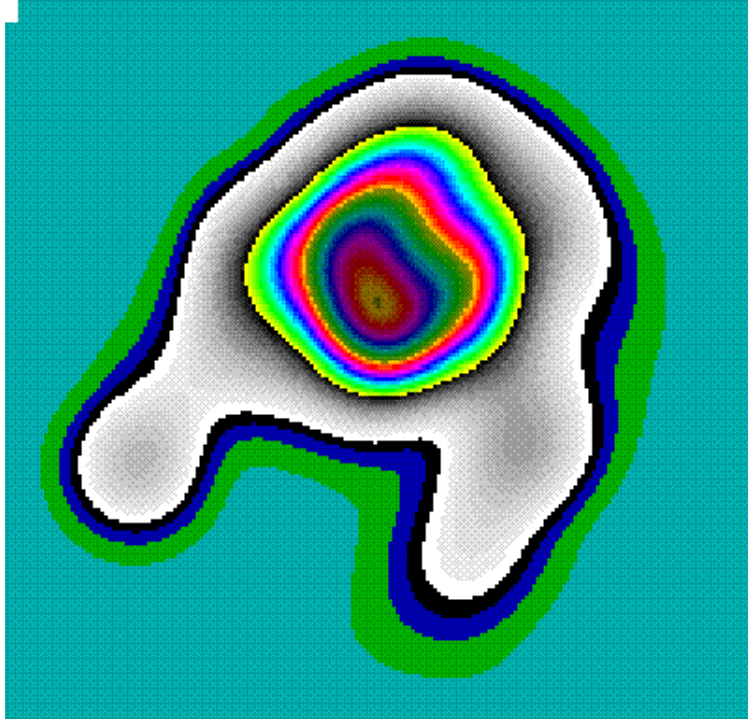


Figure 4: The raw data of Figure 1 observed with a 20 m dish.

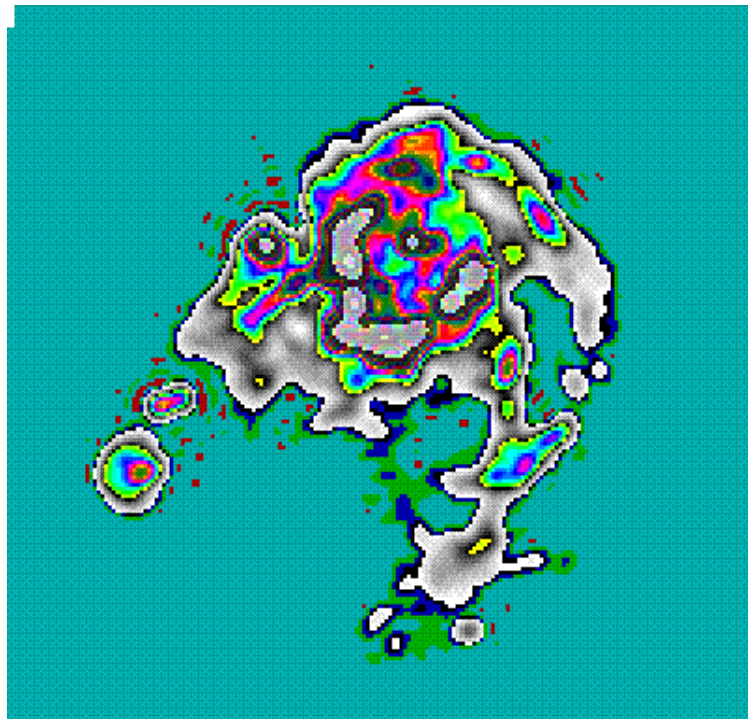


Figure 5: The combination of interferometric data from Figure 2 with single dish data from Figure 3 or Figure 4. In the absence of noise and pointing or other errors, the combination using 8m single dish data is identical to that using 20m data.

Figs 1 to 5 show an example of intermediate steps of the simulations.

Fig 1 shows the original model source distribution. Fig 3 shows the source as it would appear observed with an 8m dish, in the absence of noise and pointing errors, while Fig 4 shows the source observed with a 20m dish, also in the absence of noise and pointing errors. Fig 2 shows the source observed with the MMA in its compact configuration, with a maximum baseline of 70m, using only interferometric data and hence with missing short spacing information. Fig 5 shows the combination of the interferometric data of Fig 2 and the data of either Fig 3 or Fig 4. In the absence of noise, pointing and other errors, the combination of interferometric data with an 8m dish and with a 20m dish is identical. This result shown in Fig 5 is indistinguishable from the original model distribution shown in Fig 1, apart from minor low level fine scale features caused by the truncation at a radius in the UV plane of 70m.

In this study the effects of different pointing errors on the reconstruction are studied, in the presence of noise. The pointing error model has the following terms; these terms may varied independently.

- (i) A systematic, global pointing offset for the entire single dish map.
- (ii) A random tracking error for the single dish data.
- (iii) A systematic, global pointing offset for the entire MMA mosaic.
- (iv) A random tracking error occurring throughout each MMA pointing within the mosaic.
- (v) A systematic random offset of each pointing of the MMA observation, remaining constant for the duration of each individual pointing, affecting all MMA antennas equally, but varying randomly from one pointing to the next. This is representative of an important class of pointing error that might affect all dishes equally, such as an uncorrected change in refraction coefficient between a calibration measurement and the observations.

These terms are considered to be a useful representation of the variety of pointing errors encountered in single dish or interferometric modes of observation.

The Phase Fitting algorithm

Interferometer observations made with 8m diameter antenna elements, and with a closest element separation of 9m, in principle contain information on baselines down to 1m, albeit with vanishing weight. Since an 8m diameter antenna in single dish mode measures data out to a radius of 8m in the UV plane, there is at least in principle a significant overlap of UV coverage. This is illustrated in Fig. 6.

Total power observations made with a 20m dish of course give a greater overlap in UV coverage, illustrated in Fig. 7. A Fourier Transform of the total power map made by a single dish yields a UV map; if there is a global pointing offset of the total power map, then this corresponds to linear phase gradient across the UV map. Pointing errors in the antenna elements used for interferometric measurements do not, to a good approximation, affect the phase in the UV plane. By comparing the phase in UV space between the single dish data and the interferometric data, it should be possible to measure the linear phase gradient resulting from the single dish pointing error. The success of this process is limited primarily by signal-to-noise ratio in this region of UV overlap.

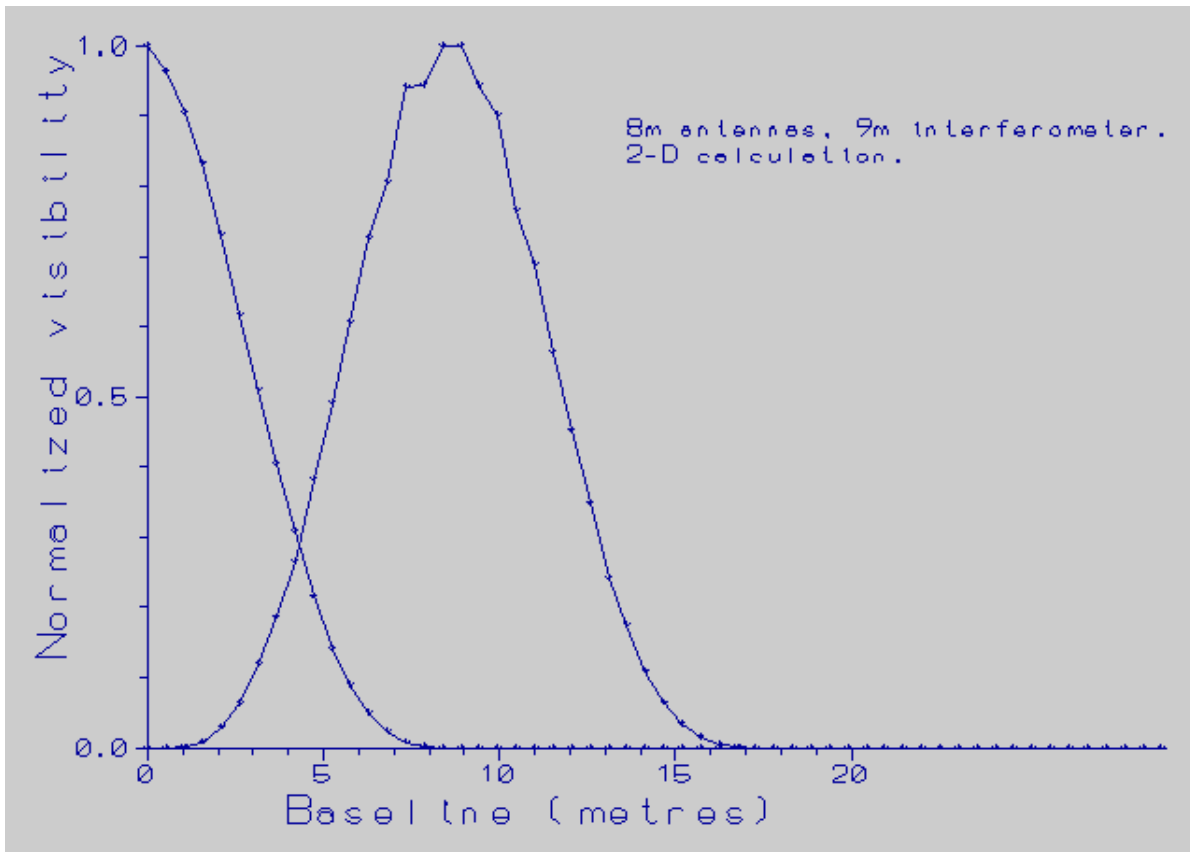


Figure 6: Radial profile from a calculated 2-D spatial frequency response of an 8m dish in total power mode, and two 8m dishes operating as an interferometer with a 9m baseline.

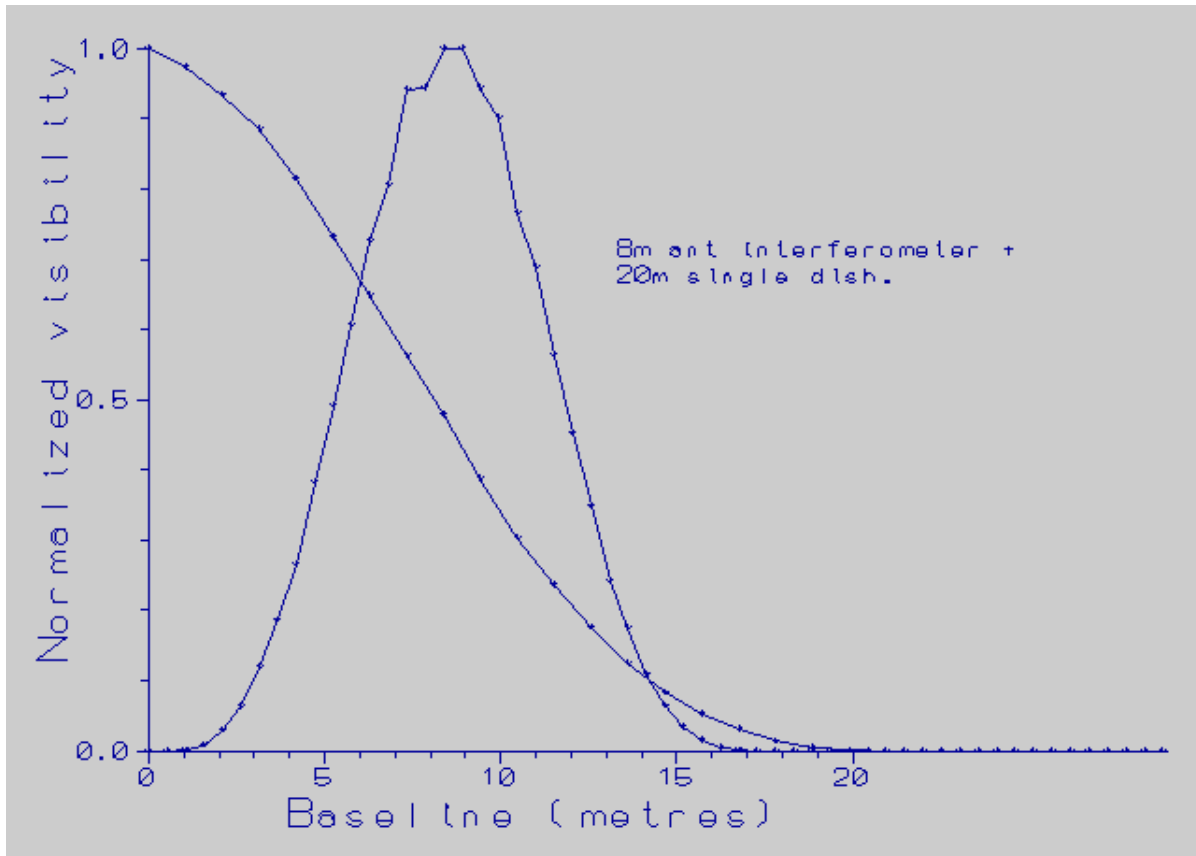


Figure 7: Radial profile from a calculated 2-D spatial frequency response of a 20m dish operating in total power mode, and an interferometer consisting of two 8m dishes spaced by 9m.

In practice the pointing error measurement and correction might be made in the following way; note that steps (i) to (iv) below are equivalent to performing a cross-correlation between the sky-plane maps of the single dish and of the interferometer data, and measuring the precise position of the central peak in the cross-correlation distribution:

- (i) create a phase map in UV space from the Fourier Transform of the single dish.
- (ii) create a phase map in UV space from the complex visibility functions measured by the interferometers.
- (iii) subtract these two phase maps.
- (iv) fit a linear inclined plane to the difference using a weighted least squares technique. The weighting will take into account the different spatial frequency response of the single dish and interferometric observations, essentially as shown by the overlap regions of Figs 6 or 7.

(v) the fitted inclined plane is subtracted from the single dish UV phase map, thereby correcting for the global pointing offset of those measurements.

Step (iv) has to consider the two-pi ambiguities of the phase map. A convenient practical implementation of the above scheme would be, for step (iv), to take a Fourier Transform using the amplitude given by the weighting function and the phase given by the phase difference map. The offset from the origin of the peak amplitude in the resulting transformed map - the "pointing error map" - gives the global pointing offset of the single dish observations with respect to the interferometer phase, as required. This also could have been derived from a direct cross-correlation between the two data sets, but additional spatial frequency filtering has been included to enhance the signal-to-noise ratio. The derived offset is then applied to the raw single dish data either as a shift in the sky plane or as an added phase gradient in the UV plane. This implementation was used for the simulations described here. Fig 8 shows a "pointing error map" made in this way, using the weighted overlap of UV response of the interferometers and observations with a 20m dish. A moderate degree of noise has been added to the data. The offset from the origin of the dominant peak in this map gives the simulated single dish global pointing error, in this case an arbitrary 10". With extremely high noise level, it may be impossible to identify the dominant peak, and the algorithm fails. This is illustrated later with Figs 9 - 14 and 19 - 20. Fig 9 shows a simple source, with noise added, as might be observed by the MMA using a 20m single dish and interferometer baselines from 9m to 30m, with no pointing errors. Fig 10 shows the effect if the single dish is mispointed by 10" (the 20m beamwidth is 16") and remains uncorrected. Fig 11 shows the result after applying the PHFIT algorithm to correct for the global pointing error; there are now no residual errors attributable to the original poor pointing.

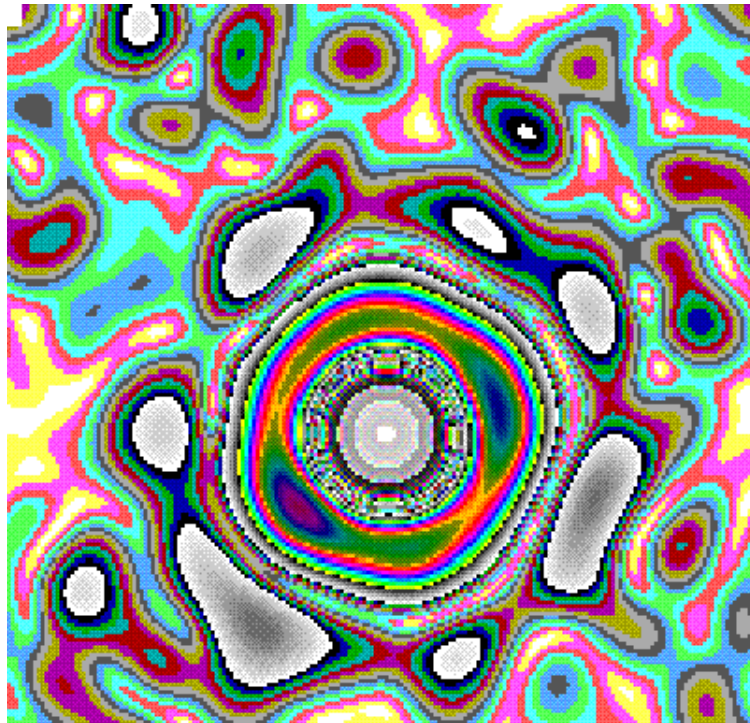


Figure 8: The "Pointing error" map, derived from the Fourier Transforms using the difference phase map of the MMA interferometric and 20m single dish data, and amplitude of the product of the UV responsivity functions illustrated in Figure 6.

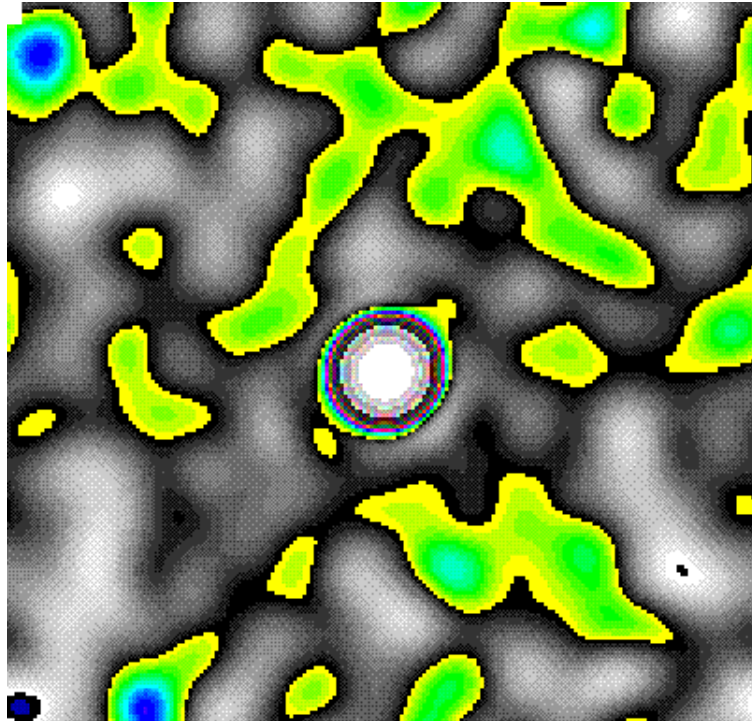


Figure 9: A simulated point source with noise, MMA out to 30 m baselines, using 20m single dish data. No pointing errors.

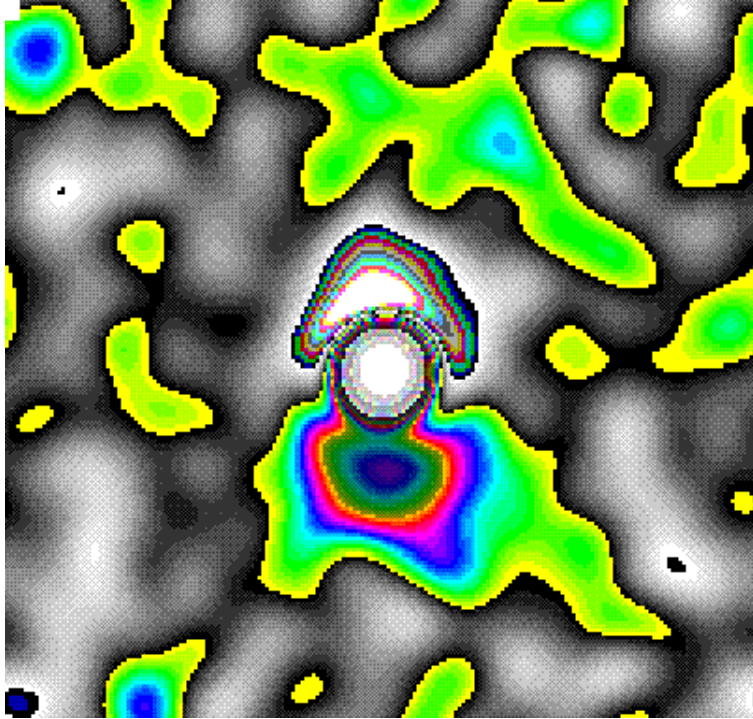


Figure 10: Simulated point source with noise, MMA to 30m baselines, using 20m single dish with 10" uncorrected pointing error.

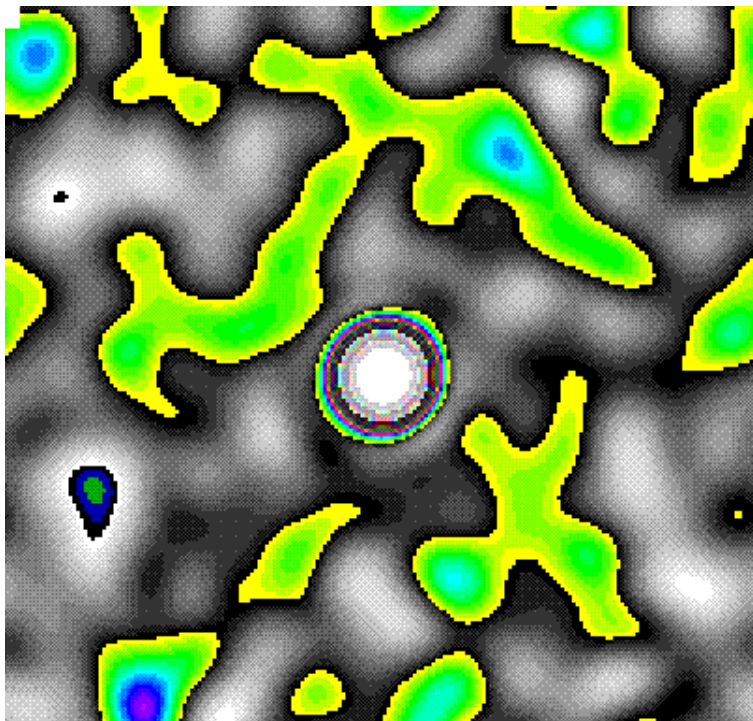


Figure 11: Simulated point source with noise, MMA to 30m, 20m dish with 10: pointing error, corrected using PHFIT.

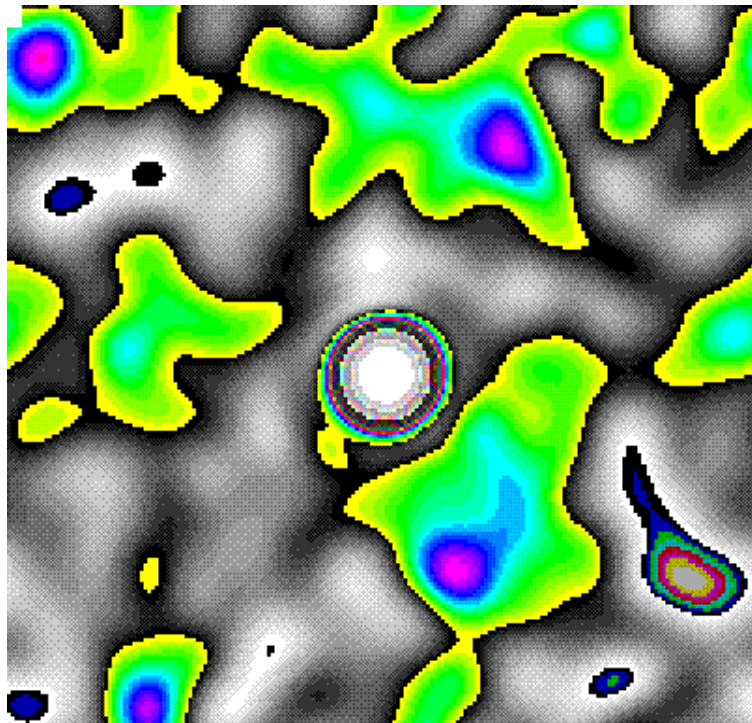


Figure 12: Point source with noise, MMA to 30 m baselines, using 8m single dish with no pointing errors.

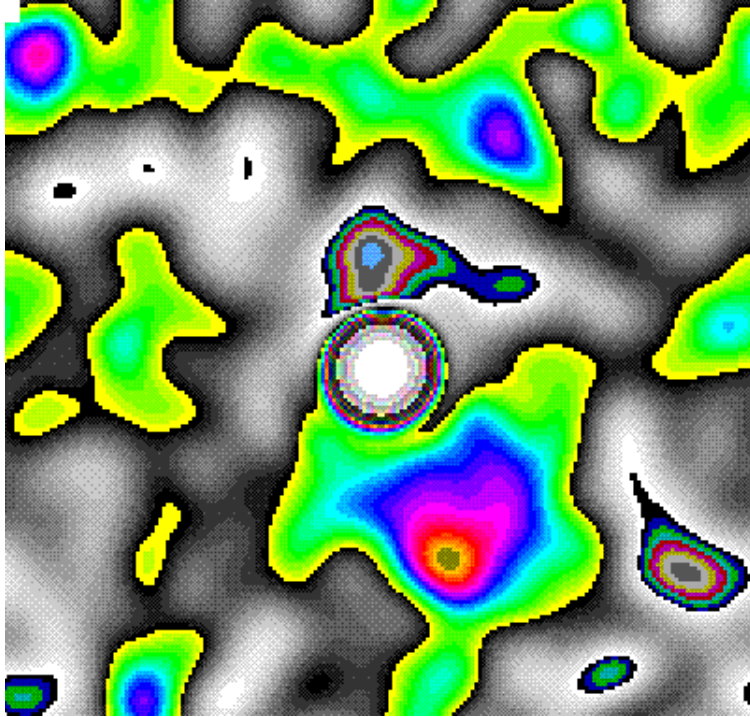


Figure 13: Point source with noise, MMA to 30m baselines, using 8m with 10" uncorrected pointing error.

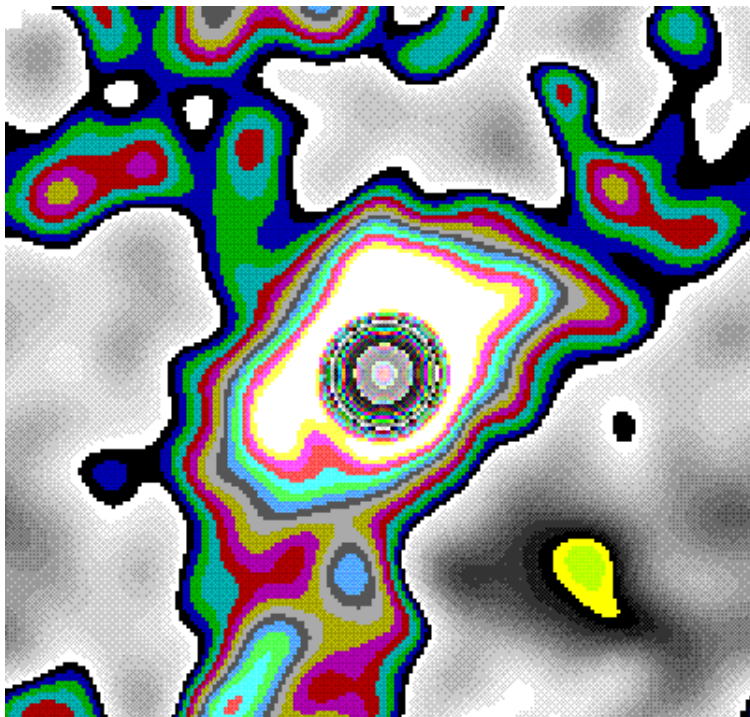


Figure 14: Point source with noise, MMA to 30m baselines, using 8m single dish with unsuccessful correction of 10" pointing error. Noise level is too high for PHFIT to operate successfully.

The threshold for failure of this technique, due to excessive noise, is higher for combinations using 20m single dish data than for 8m data. This is to be expected from Figs 6 and 7; the degree of deconvolution and the areas of overlap are both more favourable for observations using a 20m dish. Figs 19 and 20 illustrate this quantitatively. Figs 12 - 14 show the same source as Fig 9, but using an 8m dish for the short spacing data. The noise added for the examples of Figs 9 - 14 is at the same level, but is too high for PHFIT to operate successfully with 8m data, although still within the useful range for 20m data. Fig 13 shows a small negative region close to the source, caused by the uncorrected 10" pointing error in the 8m single dish data. The dominant peak of the "pointing error map" equivalent to Fig 8 has become masked by excessive noise. In this example, PHFIT degrades the resultant image (Fig 14) and is inappropriate without further refinement. However, in the uncorrected image of Fig 13 the defects due to poor single dish pointing are nearly masked by the excessive noise level, and would be invisible if MMA data were included out to 70m or more, rather than being truncated at 30m as in this example.

Figs 19 and 20 show the residual pointing errors to be expected from the PHFIT algorithm in determining the global pointing offset of the single dish data, as a function of noise level. Fig 19 shows the fitted errors where the observations are of a single point source. In this plot, a noise rms of 1.0 along the X-axis is approximately 1.2% of the peak amplitude of the point source when observed with a maximum baseline of 70m. Beyond the last points plotted - i.e. >0.5 in rms noise level for the 8m case and >2 for a 20m dish - the algorithm breaks down, as explained above. As well as having a higher threshold tolerance to noise, the residual 20m pointing error is several times smaller than the corresponding 8m residual error. Fig 20 shows the results for the model M31S source. Here 1.0 on the noise axis corresponds to 28% of the peak amplitude of the source observed with a 70m maximum baseline. This example is of much more practical relevance than the point source example, and interestingly then the difference between 8m and 20m dishes is less pronounced. The probable reason for this change is that the spatial frequency response of the source biases the useful region of UV overlap towards lower spatial frequencies, so that the extended area of overlap with the 20m dish becomes of less significance.

The effect of these errors due to imperfect operation of the PHFIT algorithm has to be put in the correct perspective. From Fig 20, the point at which PHFIT breaks down is at a signal-to-noise ratio (Peak/rms), using all baselines out to 70m, of only 4:1. Immediately below this threshold, the residual PHFIT error is approximately 3.5" for the 8m case, and less for the

20m case. Fig 15 or Fig 17 show that a 3.5" single dish global pointing error results in a degradation of dynamic range of noiseless data to about 100:1; i.e. the degradation in effectiveness of PHFIT due to noise gives image defects that are more than an order of magnitude below the noise level itself. Naturally these defects become more serious if the data are smoothed to lower resolution, thereby reducing the effective random noise level.

The simulations

Figs 15 - 18 show plots of dynamic range, as defined above, for different types of pointing error.

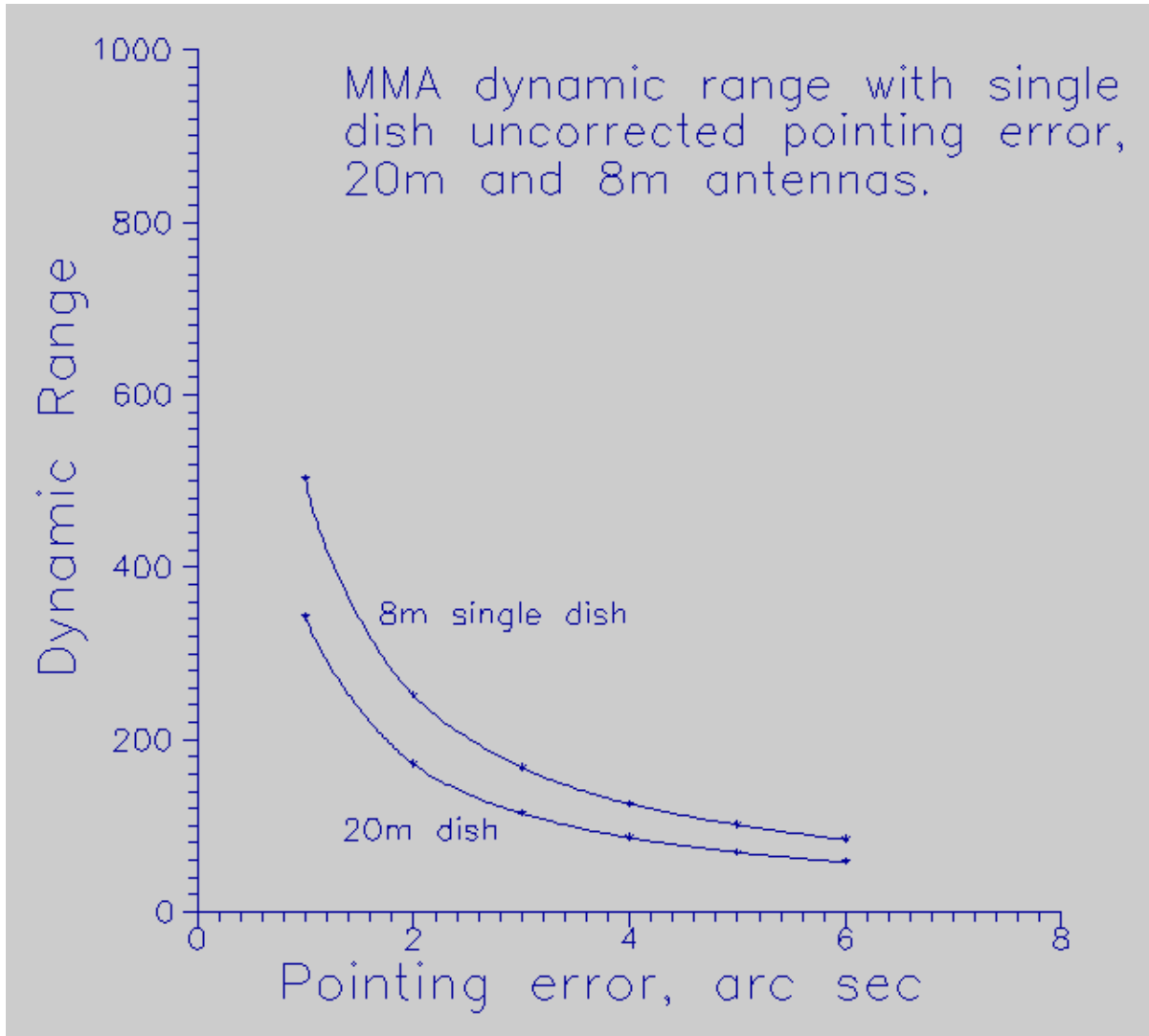


Figure 15: Dynamic range of simulated observations, as a function of single dish global pointing error, for 8m and 20m antennas. No errors in MMA interferometric observations.

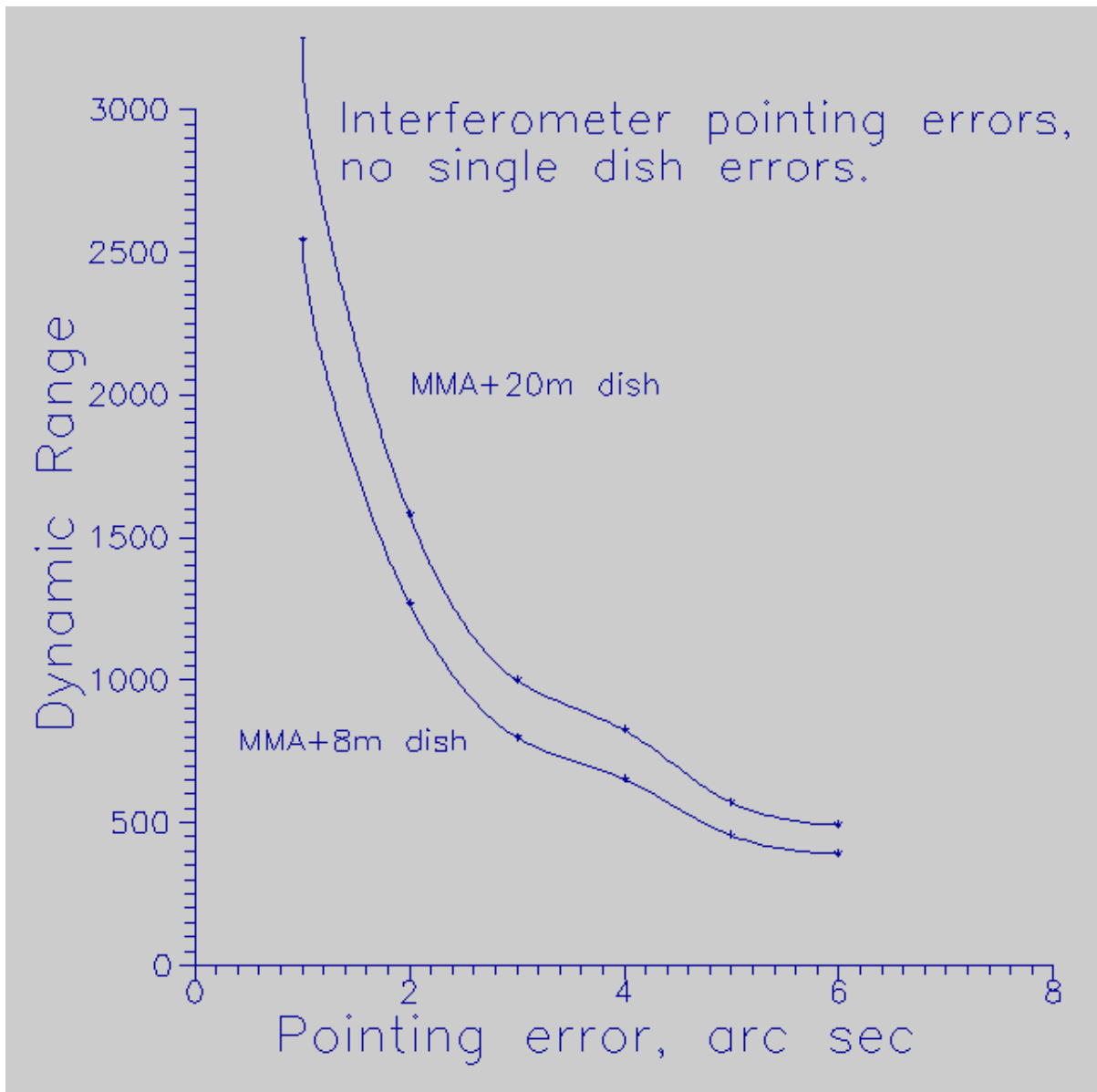


Figure 16: Dynamic range vs. MMA interferometer pointing errors, with no single dish errors.

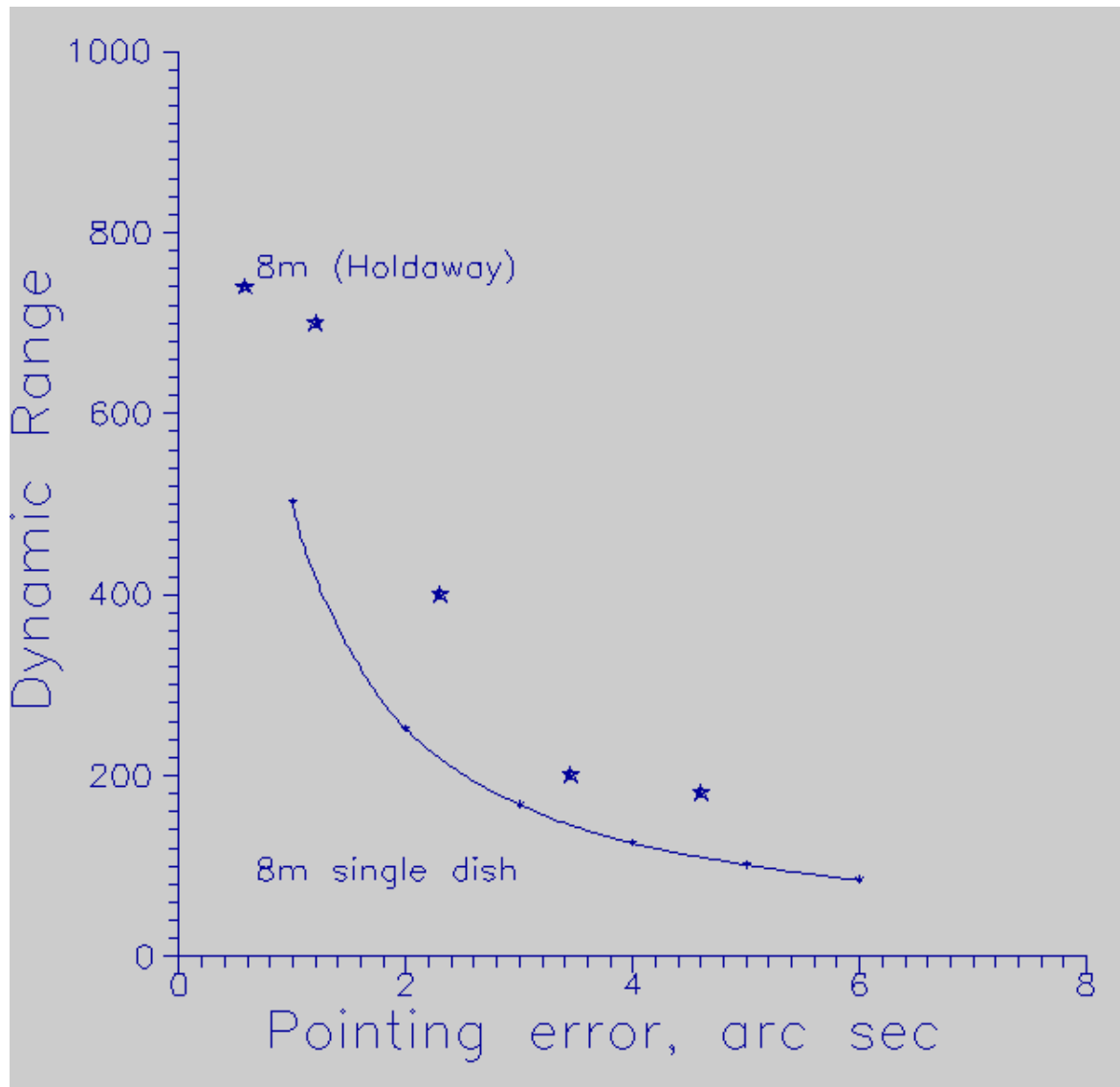


Figure 17: Comparison of this work with Holdaway (1990). The dynamic range is plotted from the current simulations, using an 8m dish for the short spacing data, as a function of pointing error.

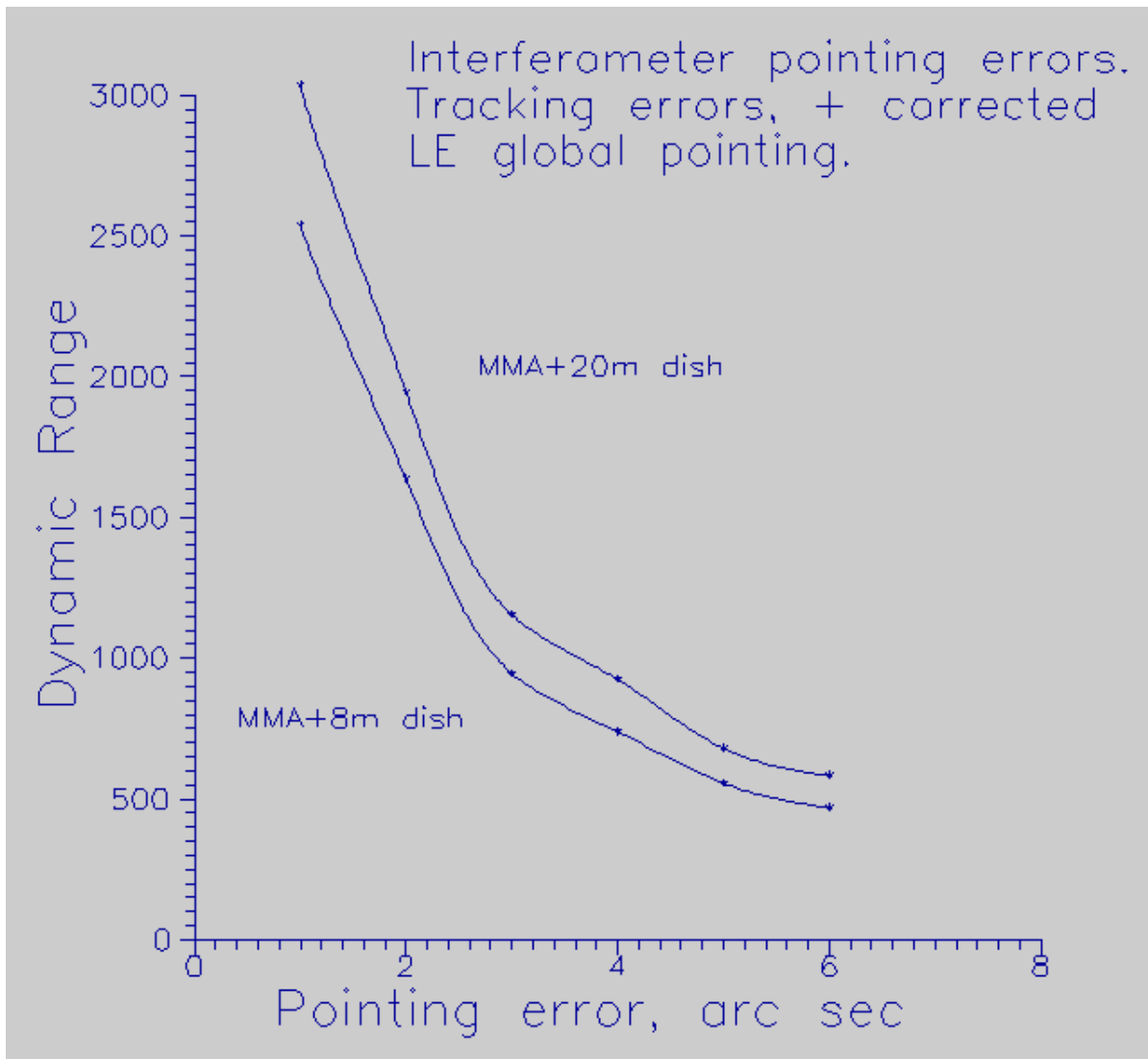


Figure 18: Dynamic range as a function of interferometer pointing error, with corrected LB global offset, including tracking and other errors.

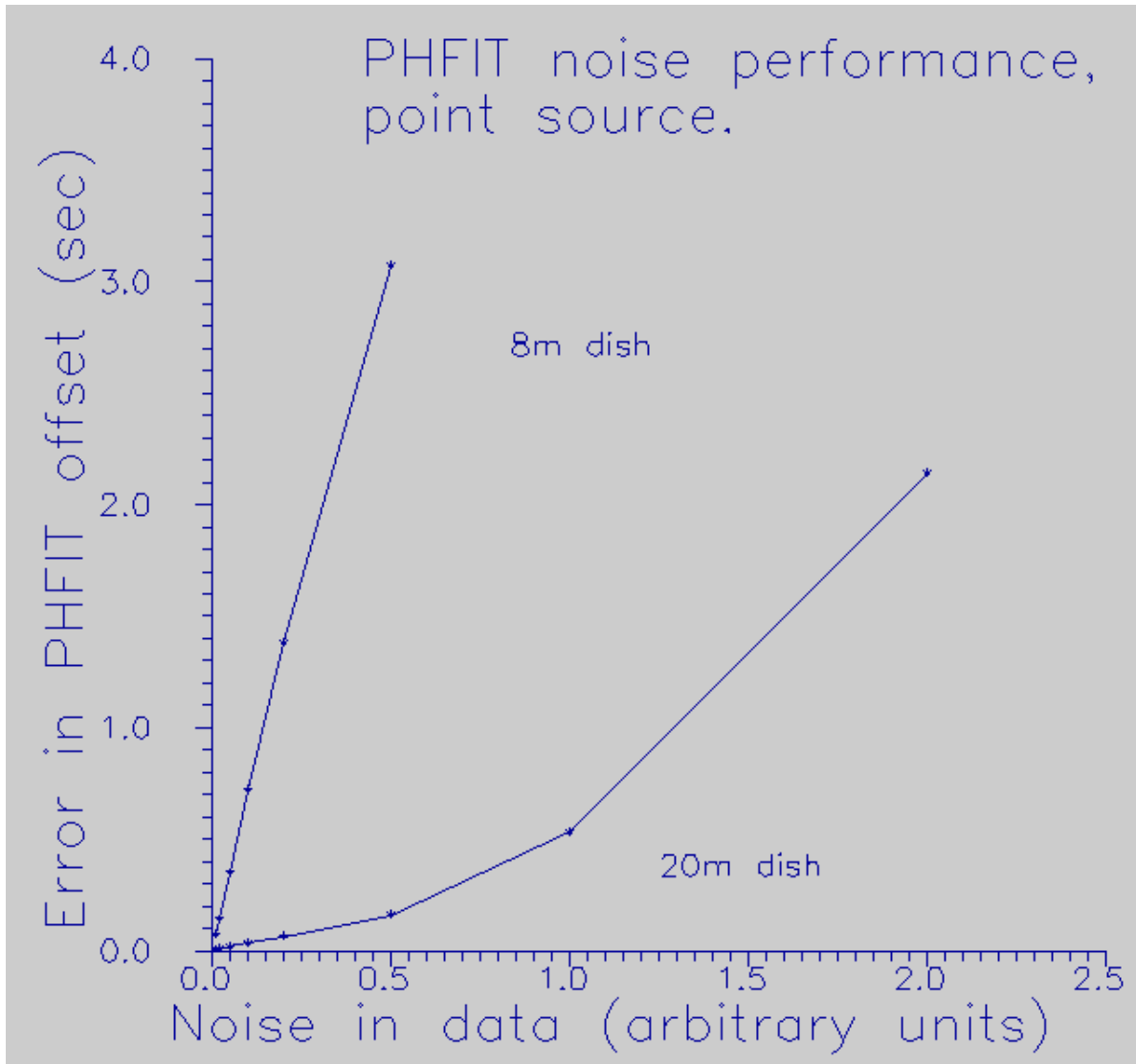


Figure 19: Error in fitting single dish global pointing offset using the PHFIT algorithm for a model point source, as a function of noise level. 8m and 20m dish data compared.

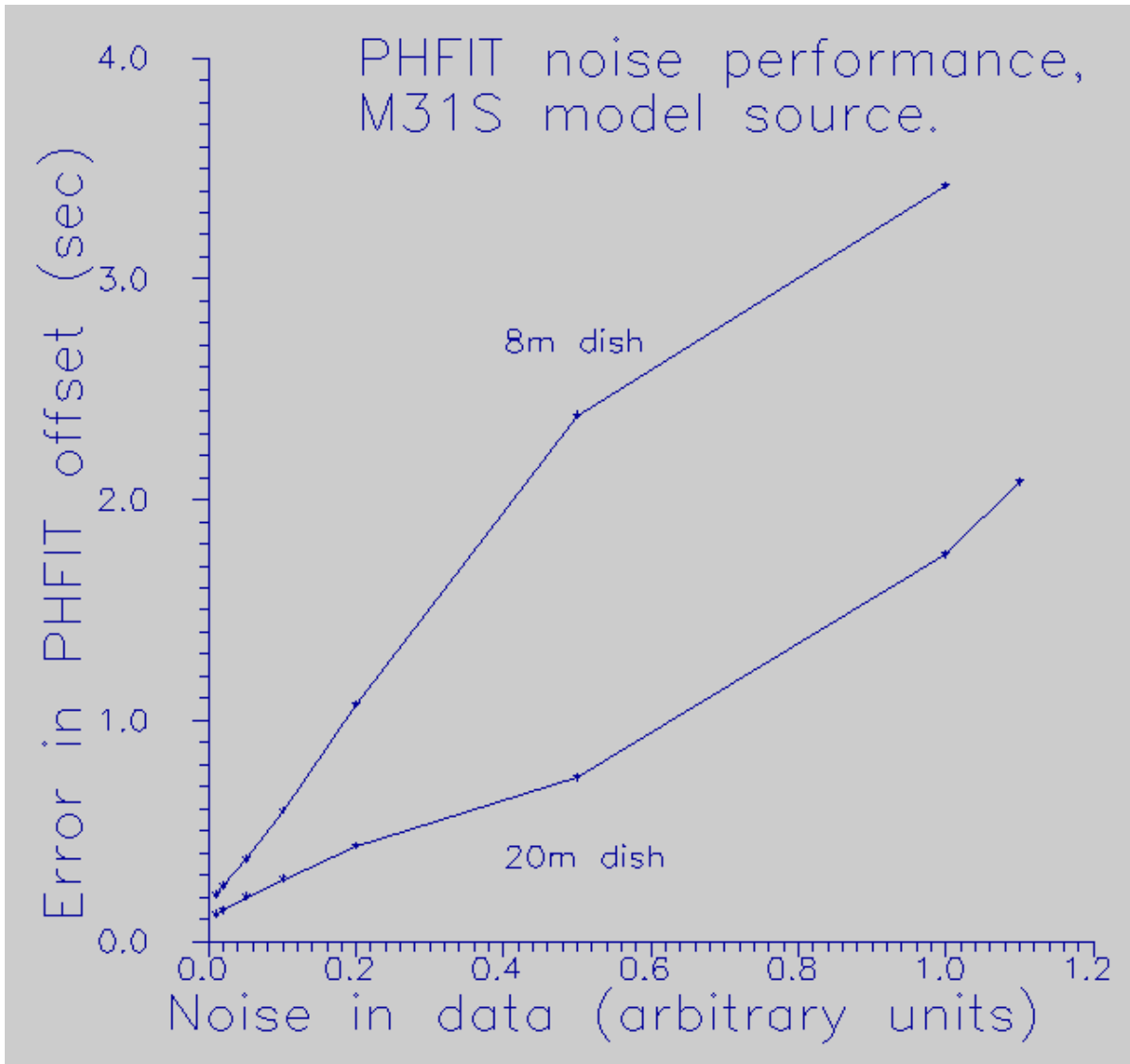


Figure 20: Error in fitting single dish global pointing error using PHFIT algorithm for the model source M31S, as a function of noise level.

Fig 15 shows the dynamic range achieved in this study with uncorrected global pointing errors in the single dish data, but with no errors in the interferometer data. Here, as earlier studies showed, for a given pointing error the larger single dish actually gives worse dynamic range.

Fig 16 shows the equivalent data where there are no single dish pointing errors, but with interferometer antenna pointing errors. Here the larger single dish gives a slightly higher dynamic range. This is to be expected, since corrupted interferometer data is given lower weight at radii smaller than 20m in the UV plane. The dynamic range is degraded about 6 times less seriously from interferometer pointing errors, than from single dish errors, for the same pointing inaccuracy.

As a comparison with earlier work, Fig 17 shows dynamic range achieved in this study as a function of pointing error, using an 8m dish for short spacing information, compared with the results shown by Holdaway in ref. (1). A slightly worse dynamic range is achieved in the current work, but considering the different assumptions of both independent simulations and the differing pointing models, the agreement is considered to be extremely good.

Fig 18 shows the result of simulations with short spacing data provided with an 8m antenna and a 20m antenna, using the following parameters:

Single dish data: 6" global pointing offset,

1" random tracking errors.

PHFIT pointing correction algorithm applied.

Sampling in sky plane better than Nyquist rate.

Interferometer data: 6" global pointing offset, identical for each pointing of the mosaic,

1" random tracking error,

a randomly different systematic pointing offset for each pointing of the mosaic away from its nominal position, varying from 0" to 6".

Adequate sampling in UV plane, for all pointings of the mosaic.

With these parameters, even with a pointing error as high as 6", a dynamic range of a little over 500:1 is achieved with a 20m single dish, and a little under 500:1 with the 8m dish providing short spacing data. For pointing errors as small as 1", a dynamic range of several thousand is obtained.

Limitations

These simulations have only explored a tiny volume of the potentially important parameter space, and like all simulations involve several important initial assumptions and approximations. One important area that has been neglected is the effect of shadowing between adjacent dishes. With the assumed minimum baseline used here of 9m, shadowing would begin at elevations **below 63 degrees**. Increasing the minimum baseline would minimize shadowing, but decrease the effectiveness of an 8m element in providing all the necessary short-spacing data in the presence of noise and other errors. This aspect of the MMA design needs study.

Conclusions

The following conclusions are drawn:

1. Where similar parameters of noise and pointing errors have been used, the predicted dynamic range vs. pointing errors from this study is in good agreement with earlier work (ref (1)).

2. Independent investigation of different pointing error components (global, differential systematic, random) shows that the dominant components regarding degradation of dynamic range are:

(a) For single dish data, using either the 8m elements in total power or a separate 20m large element (LE), global map pointing offsets dominate the effective reduction in dynamic range.

(b) For interferometric measurements, the differential systematic pointing error, i.e. the pointing error of one field of the mosaic with respect to its neighbours, is the dominant source of error.

A given uncorrected pointing error in short spacing data, derived either from a 20m or an 8m antenna element, is more harmful than the same pointing affecting interferometric data, by a factor typically of 4 to 6, depending on circumstances. If not corrected, a given global pointing error on 20m single dish is much more harmful than the same angular pointing error on an 8m dish. This had already been shown in the earlier studies.

3. The effect of the global pointing error of single dish observations, either with the 8m dishes or a separate 20m dish providing the short-spacing data, can effectively be eliminated by making use of the overlap in the UV plane of regions common to both single dish and interferometric data. This technique is very effective, and probably should be applied as a standard correction to most combined single dish and interferometric data sets. In the presence of a poor signal-to-noise ratio, the technique degrades more rapidly with a smaller single dish and its smaller area of UV plane overlap with interferometric data, than with a large single dish element.

4. if the phase overlap correction technique is applied, the 20m single dish always gives greater dynamic range in the combined MMA image than a corresponding 8m dish in total power mode. However, the difference is often marginal.

References:

(1) M. Holdaway (1990), "Imaging characteristics of a homogeneous millimeter array", NRAO Millimeter Array Memo No. 61.

(2) R. Braun (1988), "Mosaicing with high dynamic range", NRAO Millimeter Array Memo No. 46.

(3) "The Millimeter Array", Proposal to the National Science Foundation submitted by Associated Universities, Inc., July 1990, Chapter IV.